RIPK3-Mediated Necroptosis Drives Macrophage Infiltration and Corneal Neovascularization After Alkali Burn

Yue Li,[1] Boyu Yang,[2] Qi Chen,[1] Yuchen Zhou,[1] Wen Hu,[1] Xiaojia Huang,[1] Guangyi Huang,[1] Ningning Tang,[1] Fen Tang,[1] Hui Huang,[1] Qianqian Lan,[1] Wenjing He,[1] Fan Xu,[1] Yiming Ye,[2] and Li Jiang[1]

[1]Department of Ophthalmology, The People's Hospital of Guangxi Zhuang Autonomous Region, Guangxi Key Laboratory of Eye Health, Guangxi Health Commission Key Laboratory of Ophthalmology and Related Systemic Diseases Artificial Intelligence Screening Technology, Institute of Ophthalmic Diseases, Guangxi Academy of Medical Sciences, Guangxi, China
[2]State Key Laboratory of Ophthalmology, Zhongshan Ophthalmic Center, Sun Yat-Sen University, Guangdong Provincial Key Laboratory of Ophthalmology and Visual Science, Guangzhou, China

Correspondence: Li Jiang, Department of Ophthalmology, The People's Hospital of Guangxi Zhuang Autonomous Region, Guangxi Key Laboratory of Eye Health, Guangxi Health Commission Key Laboratory of Ophthalmology and Related Systemic Diseases Artificial Intelligence Screening Technology, Institute of Ophthalmic Diseases, Guangxi Academy of Medical Sciences, 6 Taoyuan Rd., Nanning, Guangxi 530000, China; eyejiangli@163.com.
Yiming Ye, State Key Laboratory of Ophthalmology, Zhongshan Ophthalmic Center, Sun Yat-Sen University, Guangdong Provincial Key Laboratory of Ophthalmology and Visual Science, 7 Jinsui Rd., Guangzhou 510060, China; yym1816@qq.com.
Fan Xu, Department of Ophthalmology, The People's Hospital of Guangxi Zhuang Autonomous Region, Guangxi Key Laboratory of Eye Health, Guangxi Health Commission Key Laboratory of Ophthalmology and Related Systemic Diseases Artificial Intelligence Screening Technology, Institute of Ophthalmic Diseases, Guangxi Academy of Medical Sciences, 6 Taoyuan Rd., Nanning, Guangxi 530000, China; oph_fan@163.com.

YL, BY, QC, YZ, and WH contributed equally to the work presented here and should therefore be regarded as equivalent authors.

Purpose. To reveal the role of receptor-interacting protein kinase 3 (RIPK3) in regulating macrophage inflammation and corneal neovascularization (CoNV) induced by alkali burn.

Methods. A corneal alkali burn (AB) model was established in C57BL/6J (wild-type) and RIPK3$^{fl/fl}$Cx3cr1$^{+/cre}$ (RIPK3$^{-/-}$, RIPK3 knockout [KO]) mice using sodium hydroxide. Anterior segment optical coherence tomography and hematoxylin and eosin staining were used to evaluate the impact of RIPK3 on corneal edema and morphology. CoNV was detected by slit-lamp microscopy and whole-mount immunofluorescence staining of cornea. Corneal macrophage and necroptotic cell death was analyzed through immunofluorescence staining and propidium iodide (PI) staining. Activation of the necroptosis pathway was examined after corneal AB by western blot.

Results. Necroptosis-related proteins RIPK1, RIPK3, and mixed lineage kinase domain-like (MLKL) were upregulated and activated following corneal AB. Among these, RIPK3 demonstrated the most pronounced increase. Notably, the elevated level of RIPK3 was prominently colocalized with the infiltrating F4/80^{+} macrophages. RIPK3 KO significantly alleviated corneal edema and morphology defects. Additionally, as the corneal morphological defects progressed, macrophages became activated, and CoNV and lymphangiogenesis (LyG) were enhanced. RIPK3 KO markedly reduced AB-induced macrophage accumulation, as well as CoNV and LyG. RIPK3 KO mice also showed a meaningful decrease in PI^{+} necroptotic cells. Mechanistically, AB-induced necroptosis stimulated the expression of MLKL and fibroblast growth factor 2 (FGF2), whereas RIPK3 deficiency decreased their expression.

Conclusions. This study revealed that RIPK3-mediated necroptosis drives macrophage inflammation and CoNV. Targeting RIPK3 could effectively suppress these responses by inhibiting the MLKL/FGF2 pathway, making it a promising therapeutic strategy for corneal AB.

Keywords: RIPK3, necroptosis, macrophage, inflammation, corneal neovascularization

Investigative Ophthalmology & Visual Science

iovs.arvojournals.org | ISSN: 1552-5783

Received: December 18, 2024
Accepted: May 24, 2025
Published: June 17, 2025

Citation: Li Y, Yang B, Chen Q, et al. RIPK3-mediated necroptosis drives macrophage infiltration and corneal neovascularization after alkali burn. *Invest Ophthalmol Vis Sci.* 2025;66(6):54. https://doi.org/10.1167/iovs.66.6.54

Corneal alkali burn (AB), one of the most severe forms of ocular trauma,[1] may cause significant corneal scarring and opacity even with prompt treatment and is a leading cause of blindness worldwide.[2,3] After corneal AB, the disruption of surface barrier homeostasis leads immune cells with surveillance functions to release various chemokines that specifically attract macrophages.[4] This accumulation of macrophages not only plays a central role in corneal neovascularization (CoNV) and fibrosis by releasing vascular endothelial growth factor (VEGF) and secreting interleukin-1β (IL-1β),[5,6] but also contributes to the repair of corneal injuries by phagocytosing and removing foreign bodies.[7] Furthermore, following tissue injury or infection, activated macrophages generate reactive oxygen and nitrogen intermediates that can severely damage surrounding tissues and lead to aberrant inflammation.[8] Nevertheless, the long-term anti-inflammatory outcomes for corneal AB have been disappointing; therefore, investigating the mechanisms of macrophage-mediated injury in AB may offer a therapeutic target to prevent extensive tissue damage to the cornea.

Three regulated modes of necrotic cell death in macrophages have been identified, each associated with distinct pathological outcomes: necroptosis, pyroptosis, and parthanatos.[9] Unlike apoptosis, which is generally considered "silent," necroptosis amplifies cell death and activates macrophages in response to infection or sterile inflammatory conditions.[9] This activation leads to extensive macrophage infiltration, which in turn triggers inflammation-related responses, including inflammatory CoNV and lymphangiogenesis (LyG).[10,11] Lymphatic vessels are critical for facilitating leukocyte migration and clearing inflammatory mediators back to the bloodstream, and they are typically present in most vascularized tissues.[12] The formation of new lymphatic vessels in the context of inflammation can result from the proliferation of pre-existing vessels or the growth of new lymphatic vessels.[13] Consistently, the rapid tissue penetration and severe damage caused by AB exacerbate corneal inflammation and loss of limbal epithelial stem cells, complicating cell death and regeneration.[14–16] However, the mechanisms linking AB-induced cell death to inflammation remain unclear.

Receptor-interacting protein kinase 3 (RIPK3) is a key signaling molecule in the necroptosis pathway and is essential for development, tissue injury response, and antiviral immunity.[17,18] During the abnormal activation of necroptosis, RIPK1 recruits and phosphorylates RIPK3, forming a complex known as the ripoptosome.[19] This RIPK1/RIPK3 complex then recruits and phosphorylates mixed lineage kinase domain-like (MLKL), a critical mediator of necroptotic signaling downstream of RIPK3, ultimately forming the necrosome.[19–21] Notably, necroptosis can also occur independently of RIPK1 through the RIPK1 homotypic interaction motif (RHIM)-dependent recruitment of RIPK3.[22] RIPK3/RIPK1 kinases have been shown to exacerbate macrophage inflammation and promote choroidal neovascularization.[23,24] A recent study confirmed that necrostatin-1 (Nec-1) is an effective inhibitor of RIPK1 and RIPK3,[25] demonstrating its potential in combating necroptosis-driven macrophage inflammation in atherosclerosis.[26] It has been also proved in experiments that in oxygen-induced retinopathy (OIR) mice, the hypoxia–necroptosis signaling axis promotes retinal neovascularization, whereas RIPK3 inhibition with GSK840 effectively reduces neovascularization by targeting the necroptosis pathway.[27] Moreover, previous studies have demonstrated that ultraviolet-induced corneal endothelial cell death occurs via RIPK3/MLKL-mediated necroptosis,[28] and that phenylephrine induces necroptosis in human corneal epithelial cells through the activation of RIPK1/RIPK3/MLKL signaling.[29] Thus, regulating RIPK3 function maybe a key determinant with regard to whether necroptosis drives macrophage inflammation and CoNV following AB.

In the present study, we utilized genetically engineered mice to observe the potential role of RIPK3-mediated necroptosis in regulating macrophage inflammation and CoNV in the corneal AB model.

Materials and Methods

Human Corneal Tissue Samples

Human corneal tissues were collected in accordance with the tenets of the Declaration of Helsinki. The research protocol was approved by the Institutional Review Committee of The People's Hospital of Guangxi Zhuang Autonomous Region (KY-GZR-2021-108). All surgical recipient patients and family members of all deceased organ donors provided informed consent after receiving a full explanation of the nature and potential risks of the study. Human AB corneal tissues were obtained from patients ($n = 3$; average age, 55.67 $\pm$ 10.54 years) who underwent corneal transplantation at the Department of Ophthalmology, The People's Hospital of Guangxi Zhuang Autonomous Region. Normal corneal tissues ($n = 3$; average age, 40.33 $\pm$ 7.13 years) were collected from surplus donor tissue following corneal transplantation. The human tissue experiments complied with the guidelines of the ARVO Best Practices for Using Human Eye Tissue in Research. The baseline characteristics of the patients are listed in Supplementary Table S1, and representative slit-lamp photographs of human corneas are provided in Supplementary Figure S1.

Animals

Male and female C57BL/6J mice and homozygous RIPK3$^{-/-}$ mice (RIPK3$^{fl/fl}$Cx3cr1$^{+/cre}$) were purchased from Cyagen

Biotechnology Co., Ltd. (Suzhou, China) and Shanghai Model Organisms (Shanhai, China). All mice were bred and maintained in the Animal Experiment Center of Guangxi Medical University. Animals were housed in an air-conditioned room at 22°C on a 12-hour light–dark cycle and were given standard laboratory chow and water ad libitum. All procedures were performed in accordance with the ARVO Statement for the Use of Animals in Ophthalmic and Vision Research.

Corneal Alkali Burn Model

AB was conducted as previously described.[30] Briefly, anesthesia was administered via intraperitoneal injection of 1% pentobarbital solution (0.1 mL/10 mg), and local anesthesia of the cornea was achieved using 0.5% bupivacaine hydrochloride (Alcon, Geneva, Switzerland). Under an ophthalmic surgical microscope, a 2-mm filter paper soaked in 1-N sodium hydroxide was carefully placed on the central cornea of the right eye for 40 seconds. Following this, the right cornea was rinsed with saline for 10 minutes. All mice underwent alkali injury in the right eye, and the left eye served as an uninjured control.

Immunofluorescence

For frozen section immunofluorescence, eyeballs were treated with a 30% sucrose solution overnight, embedded in optimum cutting temperature compound, and sectioned at a thickness of 8 µm. Corneal sections were incubated with primary antibodies (Supplementary Table S3), followed by incubation with corresponding secondary antibodies. Nuclei were counterstained with 4′,6-diamidino-2-phenylindole (DAPI). Confocal images were captured using a ZEISS LSM 980 microscope (Carl Zeiss Microscopy, Oberkochen, Germany). The fluorescence intensity of phosphorylated RIPK3 (p-RIPK3) and RIPK3 was quantified by calculating the average pixel intensity within the defined region of interest. Consistent threshold settings were applied across all images to ensure comparability. Background fluorescence intensity was measured and subtracted to correct for nonspecific signals. Following background correction, the mean fluorescence intensity values were normalized relative to the control group. All labeled cells were manually quantified using the Multi-point Tool in ImageJ software (National Institutes of Health, Bethesda, MD, USA).

Hematoxylin and Eosin Staining

Hematoxylin and eosin (H&E) staining was performed following standard procedures. Tissues were first fixed in 10% formalin, dehydrated through a graded series of ethanol solutions, cleared in xylene, and embedded in paraffin. Sections were cut at a thickness of 5 µm and mounted on glass slides. The slides were then deparaffinized in xylene and rehydrated through a descending ethanol series to distilled water. Hematoxylin was applied to stain the nuclei, followed by washing in running tapwater. The stained sections were then observed and imaged with a Pannoramic MIDI scanner (3DHISTECH, Budapest, Hungary).

Anterior Segment Optical Coherence Tomography

Anterior segment optical coherence tomography (AS-OCT) was conducted with a SPECTRALIS HRA+OCT (Heidelberg Engineering, Heidelberg, Germany) to obtain detailed imaging of the corneal structure and anterior segment anatomy. Prior to imaging, animals were anesthetized with a combination of intraperitoneal pentobarbital and topical anesthetic applied to the cornea to minimize discomfort. The eye was positioned using a fixation device to ensure proper alignment with the AS-OCT system. Two trained ophthalmic examiners cross-checked to ensure the detection of maximum corneal thickness.

Ocular Observations and Corneal Neovascularization Scoring

Ocular surfaces were observed under a slit-lamp microscope, and photographs were captured by a digital camera. Mice were anesthetized by intraperitoneal injection of 1% pentobarbital solution. The areas of CoNV were quantified by ImageJ. The ratio of the area in the image to the whole corneal area was used for normalization to minimize errors caused by the imaging process.[31] The CoNV scores, which were determined by assessing the intensity, length, and clock hours of the blood vessels, are detailed in Supplementary Table S2.[31]

Whole-Mount Immunofluorescence Staining of Cornea

Eyeballs were harvested and fixed after perfusion. The whole cornea immunofluorescence was used to evaluate the CoNV area and LyG area. Corneal samples were blocked in a solution containing 5% donkey serum and then incubated with primary antibodies (Supplementary Table S3) overnight, followed by corresponding secondary antibodies for another 2 hours. We cut each cornea into four wedges to facilitate subsequent photography and statistics. All samples were imaged using the ZEISS LSM 980 confocal microscope.

Propidium Iodide Staining

Frozen corneal sections were fixed with 4% paraformaldehyde, after which a propidium iodide (PI; Thermo Fisher Scientific, Waltham, MA, USA) working solution (5 µg/mL) was applied to ensure complete coverage of the tissue. The sections were incubated in the dark at 37°C for 15 minutes. Following incubation, the sections were washed three times with PBS. DAPI was used for nuclear counterstaining. All samples were imaged using the ZEISS LSM 980 confocal microscope.

Western Blot Analysis

First, four mice from each group were killed, and their corneal tissues were homogenized in ice-cold radioimmunoprecipitation assay (RIPA) buffer. Next, the lysates were centrifuged, and the supernatant was collected. Protein concentration was determined using a bicinchoninic acid (BCA) assay, and equal amounts of protein were loaded and separated by electrophoresis. After electrophoresis, the proteins were transferred onto polyvinylidene fluoride (PVDF) membranes, which were then blocked with 5% BSA for 1 hour at room temperature. Primary antibodies (Supplementary Table S3) were incubated overnight at 4°C. After washing, horseradish peroxidase (HRP)-conjugated secondary antibodies for 2 hours at room temperature.

Investigative Ophthalmology & Visual Science

Protein bands were visualized using an enhanced chemiluminescence (ECL) detection system, and ImageJ software was used to analyze the results from three experiments.

Statistical Analysis

Prism 9.2 (GraphPad Software, Boston, MA, USA) was employed to perform the statistical analyses. Experiments were conducted a minimum of three times and are presented as mean ± SEM. Statistical analyses were performed using unpaired *t*-tests and one-way analysis of variance (ANOVA) with Tukey's post hoc test. $P < 0.05$ was considered statistically significant.

Results

AB Induced RIPK3-Dependent Necroptosis Activation in Human Corneal Tissue and Mice Models

To determine whether p-RIPK3 protein levels was elevated in patients with AB, we performed p-RIPK3 and ionized calcium-binding adapter molecule 1 (Iba1) co-staining. Immunofluorescence analysis showed increased p-RIPK3 intensity within Iba1$^+$ cells in AB patients compared to non-AB donors (normal) (Figs. 1A, 1B). Additionally, the number of Iba1$^+$ cells was markedly higher in AB patients relative to non-AB donors (Figs. 1C). To further explore how AB influences necroptosis in mice, we established a short-term corneal alkali injury model.[32] After a 40-second exposure to alkali, we assessed the time-dependent expression of necroptosis-related proteins. Western blot (WB) analysis revealed the temporal dynamics of p-RIPK3, total RIPK3 (t-RIPK3), phosphorylated RIPK1 (p-RIPK1), total RIPK1 (t-RIPK1), phosphorylated MLKL (p-MLKL), and total MLKL (t-MLKL) in the cornea at 1, 3, 5, 7, and 14 days post-injury. Protein levels peaked 5 days after AB, with RIPK3 (both p-RIPK3 and t-RIPK3) showing the most substantial upregulation (Figs. 1E–H). To further specify the necroptotic inflammatory cell types involved in mice, we performed p-RIPK3/Iba1 double staining. Co-immunostaining and high-resolution confocal imaging demonstrated that necroptosis occurred predominantly in Iba1$^+$ cells (Figs. 1I–K), with p-RIPK3 mainly distributed in the cytoplasm after AB (Supplementary Fig. S2). These findings suggest that necroptosis was activated in macrophages following AB.

RIPK3 Deficiency Reduced Corneal Edema and Morphology Defects After AB

In light of the significant upregulation of p-RIPK3 observed after corneal AB, we utilized RIPK3 knockout (KO) mice to investigate its role in corneal injury. As expected, WB analysis confirmed the successful knockout of RIPK3, as evidenced by the absence of RIPK3 expression (Figs. 2A, 2B). Double immunofluorescence staining with Iba1 and F4/80 confirmed that Iba1$^+$ cells in the cornea were a subset of macrophages (Fig. 2C). After AB, RIPK3 expression in F4/80$^+$ macrophages was significantly reduced in the KO group compared to wild-type (WT) mice (Figs. 2D–F). Furthermore, representative OCT images of RIPK3 KO and control mice (Supplementary Fig. S3) demonstrated that RIPK3 deletion alone did not result in notable morphological alterations in the cornea under physiological conditions.

To further evaluate the impact of RIPK3 on AB-induced corneal edema and morphological changes, H&E staining was performed. The analysis revealed that a large corneal epithelial defect, accompanied by severe edema and extensive stromal infiltration on day 3 in the WT group, was significantly reduced in the RIPK3 KO group (Figs. 2G, 2H). Furthermore, consistent with HE staining, AS-OCT analysis in RIPK3 KO mice showed a meaningfully diminution in corneal thickness and corneal edema on day 3 after AB (Figs. 2I, 2J). These results indicated that RIPK3 KO effectively reduced AB-induced corneal edema, suggesting a protective role of RIPK3 deficiency in morphology integrity.

RIPK3 Deficiency Mitigated Macrophage Infiltration After AB

To identify the specific types of corneal infiltrating inflammatory cells observed in H&E staining (Fig. 2E), we further examined the expression of CD68, a marker for activated microglia and macrophages, and F4/80, a marker for total macrophages, in corneal frozen sections at 3 days following AB. Immunofluorescence analysis revealed a marked increase in CD68$^+$ cells and F4/80$^+$ cells after AB. Notably, the number of CD68$^+$ F4/80$^+$ colocalized cells on RIPK3$^{-/-}$ mice decreased significantly (Figs. 3A–C). Additionally, double staining for CD16, a marker of pro-inflammatory macrophages, and Iba1, a marker for microglia, further confirmed these findings. The density of CD16$^+$/Iba1$^+$ colocalized cells were also significantly lower in the stroma in the RIPK3 KO group compared to the WT group (Figs. 3D–F). These results suggest that RIPK3 deficiency significantly ameliorated alkali-induced macrophage infiltration into the corneal stroma following AB.

RIPK3 Deficiency Attenuated Pathological Neovascularization and Lymphangiogenesis After AB

It is well established that inflammation is closely associated with CoNV and lymphangiogenesis.[33–35] In our investigation of CoNV, a representative photograph indicated that the CoNV area and CoNV score were significantly reduced in the RIPK3 KO group (Figs. 4A–C). Additionally, it has been found that, during inflammation, macrophages actively contribute to the formation of new lymphatic vessels.[36] To confirm changes in CoNV and LyG after corneal AB, whole-mounted corneas were immunofluorescence stained with CD31 and LYVE-1 on day 14 post-AB (Fig. 4A, upper image), and higher magnification images were provided for clarity. Compared to the WT group, both the CoNV and LyG areas were markedly decreased in the corneas of the RIPK3 KO group (Figs. 4D–F). These results revealed that corneal AB led to a proliferative expansion of CoNV and LyG, but RIPK3 deficiency significantly mitigated these effects.

RIPK3 Deficiency Diminished Necroptotic Cell Death After AB

To assess the impact of RIPK3 on corneal necroptotic cell death following AB, we performed cell counting using immunofluorescence with PI, a dye that preferentially labels necrotic cells with compromised membrane integrity.[37] A considerable elevation in PI$^+$ necroptotic cells was observed in the corneal stromal layer after AB. However, RIPK3 KO

Investigative Ophthalmology & Visual Science

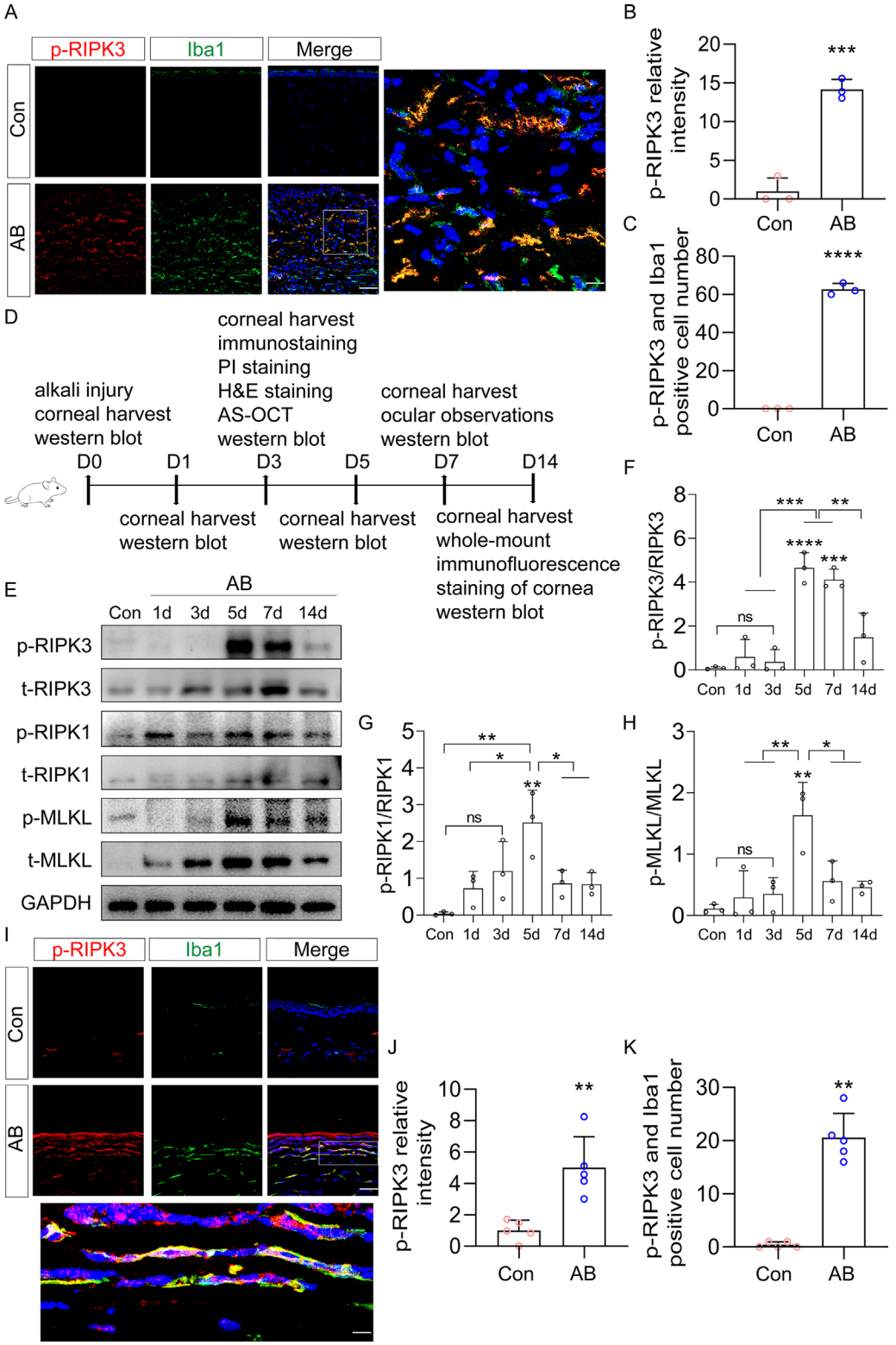

Figure 1. The necroptosis pathway was activated in both human corneal tissue and AB mouse models. Corneal tissues from normal ($n = 3$) and alkali-injured ($n = 3$) samples were collected for this study. (**A–C**) Representative images of human frozen corneal sections after corneal AB, showing co-labeling of p-RIPK3 (*red*) and Iba1 (*green*), along with quantification of p-RIPK3 staining intensity (**B**) and p-RIPK3 protein expression in Iba1$^+$ macroglia (**C**) in each group. Enlarged image is displayed on the right. *Scale bars*: 50 µm for full images; 10 µm for zoomed-in areas. (**D**) Experimental protocols. (**E–H**) Western blot analysis (**E**) and densitometry analyses (**F–H**) of p-RIPK3, t-RIPK3, p-RIPK1, t-RIPK1, p-MLKL, and t-MLKL expression in corneal samples from each group ($n = 3$). $^*P < 0.05$, $^{**}P < 0.01$, $^{***}P < 0.001$, $^{****}P < 0.0001$ (one-way ANOVA); ns, no significance. (**I–K**) Representative images showing co-labeling of p-RIPK3 (*red*) and Iba1 (*green*) (**I**), along with quantification of intensity for p-RIPK3 positive staining (**J**) and p-RIPK3 positive macroglia (**K**) in each group, 3 days after corneal AB. Enlarged image is shown below the main figures. *Blue* indicates DAPI staining. Data are presented as mean ± SEM ($n = 5$). $^{**}P < 0.01$ (Student's *t*-test). *Scale bars*: 20 µm for full images; 5 µm for zoomed-in areas.

Investigative Ophthalmology & Visual Science

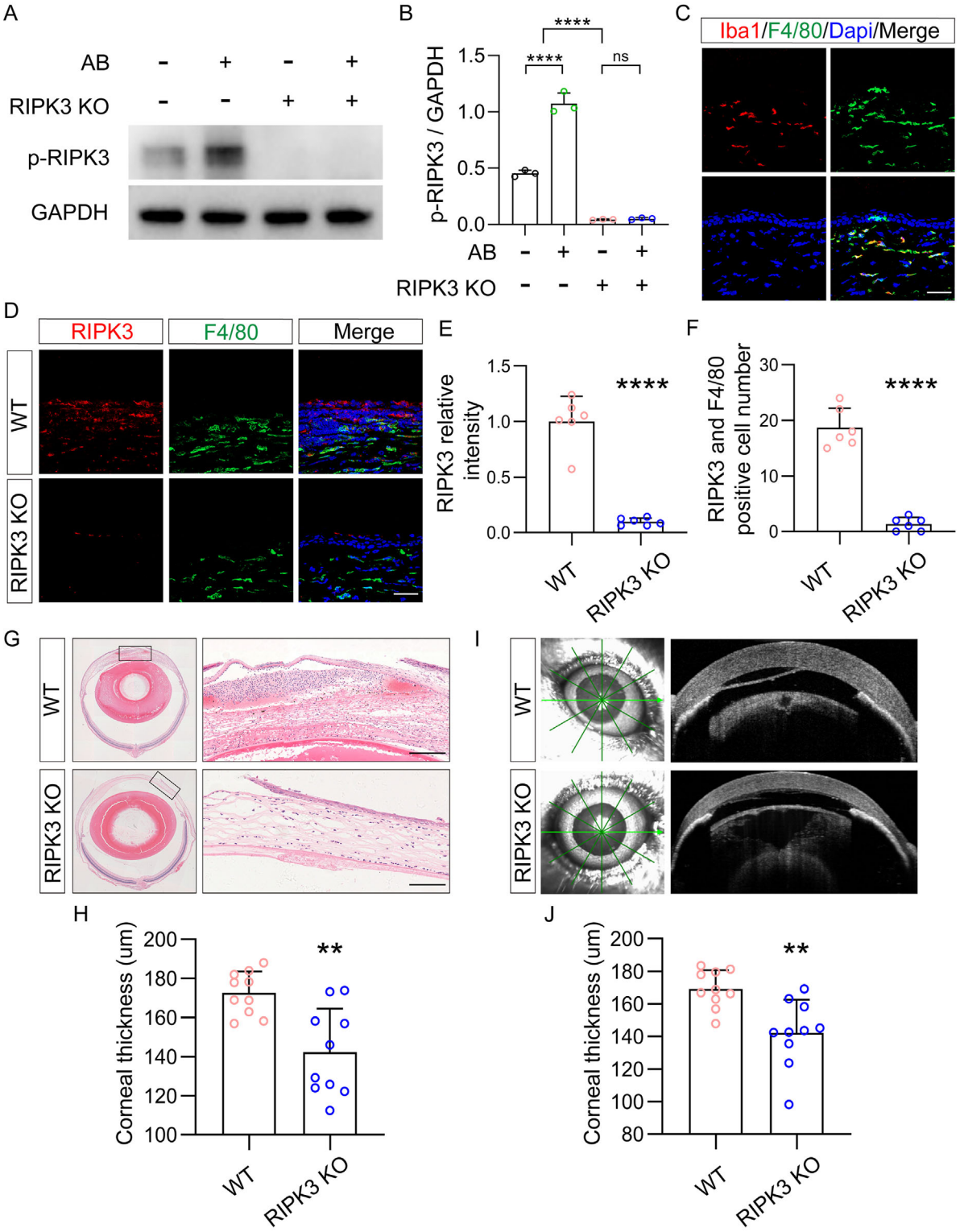

Figure 2. RIPK3 KO alleviated corneal edema and morphological defects induced by corneal AB. (**A**, **B**) Western blot analysis (**A**) and densitometry analyses (**B**) of t-RIPK3 expression in corneal samples from each group ($n = 3$). $^{****}P < 0.0001$ (one-way ANOVA); ns, no significance. (**C**) Representative images of Iba1 (*red*) and F4/80 (*green*) co-labeling in AB corneas. *Scale bar:* 20 µm. (**D–F**) Representative images of co-labeling for RIPK3 (*red*) and F4/80 (*green*) in corneal tissue (**D**), along with quantification of RIPK3 staining intensity (**E**) and RIPK3^{+} macrophages (**F**) in each group, 3 days post-corneal AB. *Blue* indicates DAPI staining. Data are presented as mean ± SEM ($n = 6$). $^{**}P < 0.01$, $^{***}P < 0.001$ (Student's *t*-test). *Scale bar:* 20 µm. *Blue* indicates DAPI staining. (**G**) Representative H&E staining images of paraffin-embedded corneal sections from WT and RIPK3 KO mice 3 days after corneal AB. (**H**) Quantification of corneal thickness in each group. (**I**) Representative high-resolution AS-OCT images of live WT and RIPK3 KO mice at 3 days after corneal AB. (**J**) Quantification of corneal thickness measured by high-resolution AS-OCT. Data are presented as mean ± SEM ($n = 10$ per group). $^{**}P < 0.01$ (Student's *t*-test). *Scale bars*: 20 µm (**C**); 100 µm (**F**); 500 µm (**H**).

Investigative Ophthalmology & Visual Science

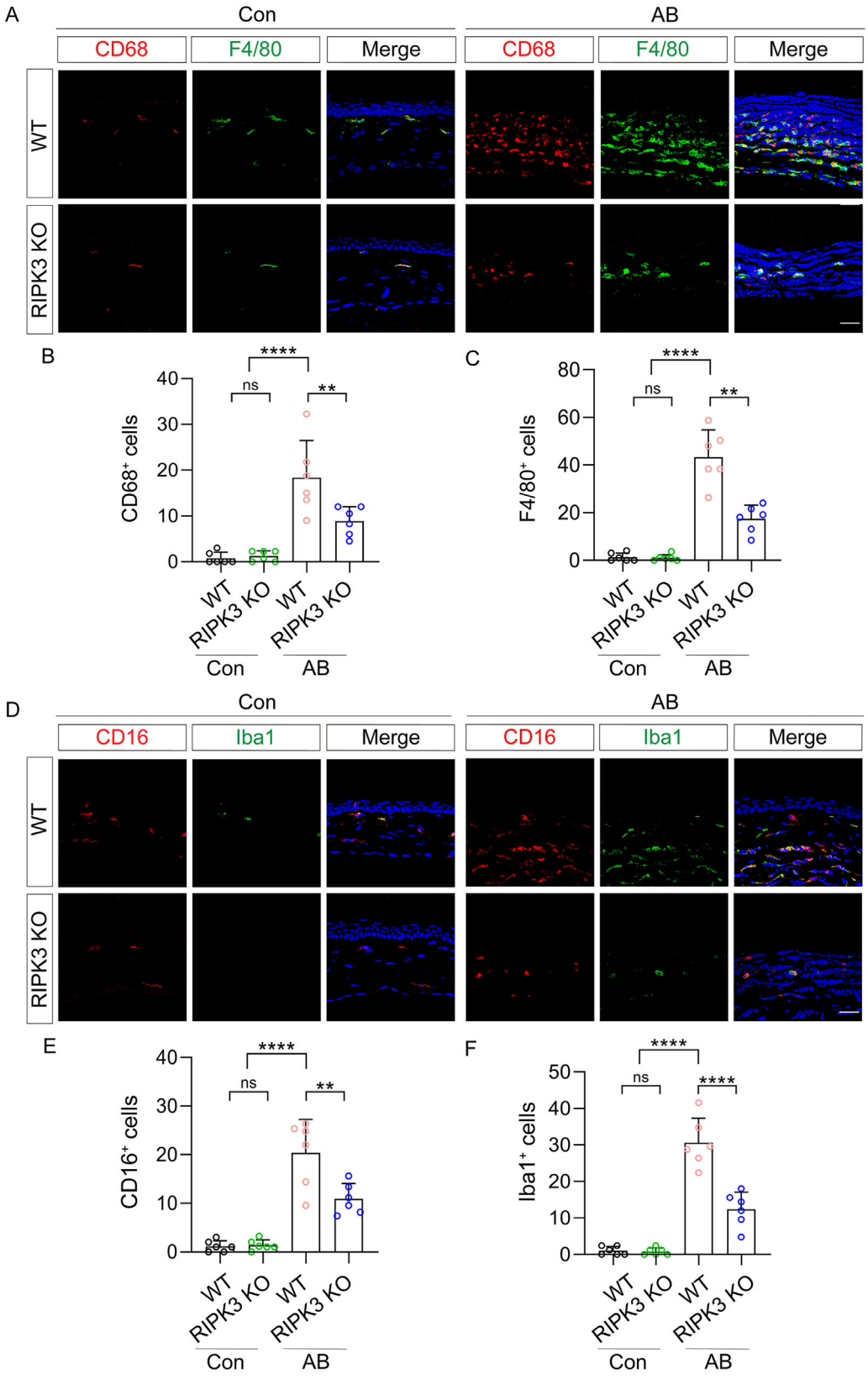

Figure 3. RIPK3 KO attenuated inflammatory responses induced by corneal AB in mice. (**A–C**) Representative images showing co-labeling of CD68 (*red*) and F4/80 (*green*) (**A**), along with quantification of Iba1$^+$ cells (**B**) and F4/80$^+$ cells (**C**) in each group, 3 days post-corneal AB. (**D**) Representative immunofluorescence images of corneal sections stained for CD16 (*red*) and Iba1 (*green*) in each group, 3 days after corneal AB. (**E**, **F**) Quantification of CD16$^+$ and Iba1$^+$ cells in each group. *Blue* indicates DAPI staining. Data are presented as mean ± SEM ($n = 6$). $^{**}P < 0.01$, $^{***}P < 0.001$, $^{****}P < 0.0001$ (one-way ANOVA); ns, not significant. *Scale bar*: 20 µm.

Investigative Ophthalmology & Visual Science

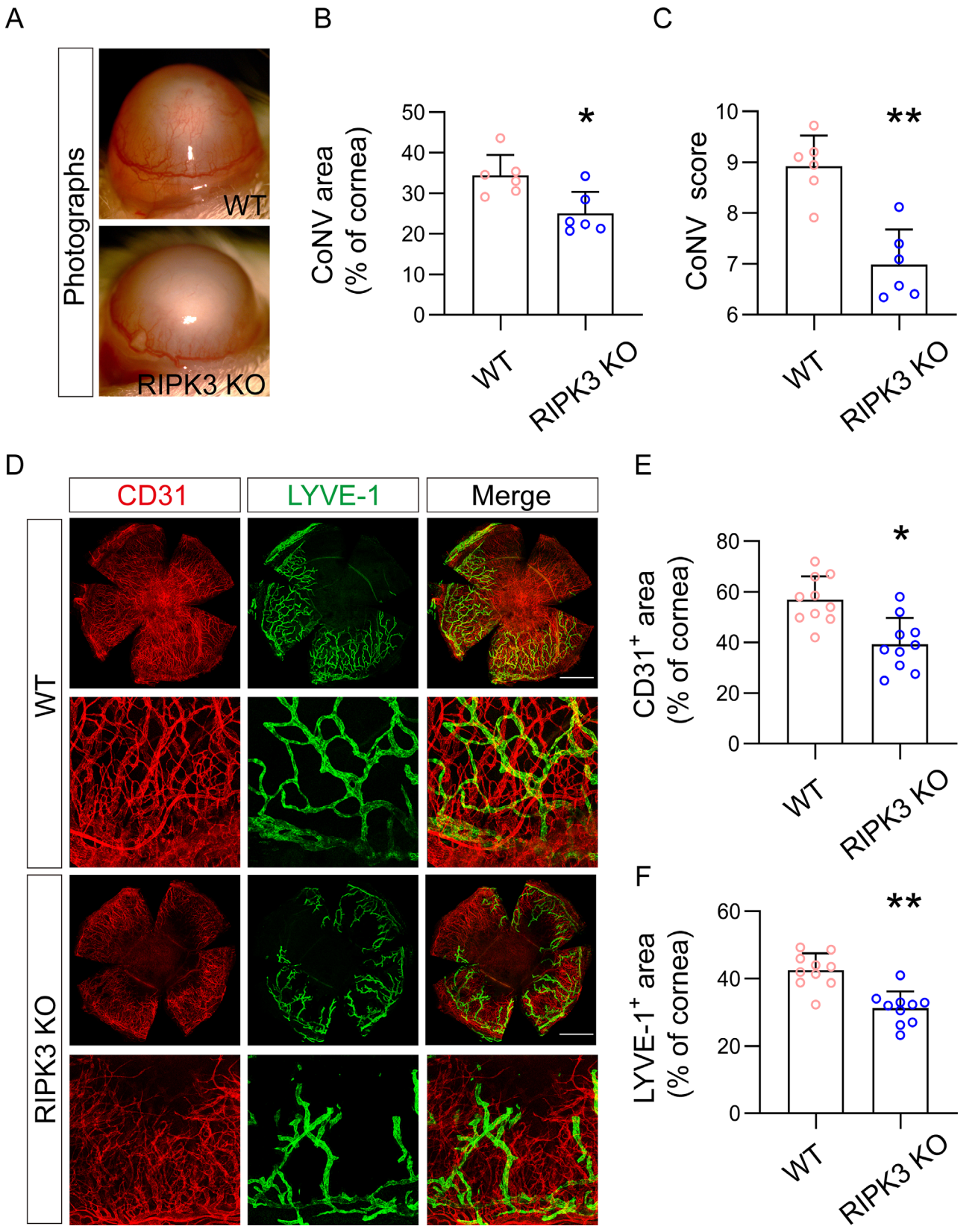

Figure 4. RIPK3 KO reduced CoNV induced by corneal AB in mice. (**A–C**) Representative slit-lamp images showing corneal neovascularization (**A**), with quantification of CoNV area (**B**) and CoNV score (**C**) in each group at 7 days post-corneal AB. Data are presented as mean ± SEM ($n = 6$). $^{**}P < 0.01$ (Student's *t*-test). (**D**) Representative immunofluorescence images of flatmounted corneas from WT and RIPK3 KO mice at 14 days after corneal AB, stained for CD31 (*red*) and LYVE-1 (*green*). (**E**, **F**) Quantification of $CD31^+$ area (**E**) and $LYVE\text{-}1^+$ area (**F**) in each group ($n = 10$). Data are presented as mean ± SEM. $^{*}P < 0.05$, $^{**}P < 0.01$ (Student's *t*-test). *Scale bar*: 500 µm.

Investigative Ophthalmology & Visual Science

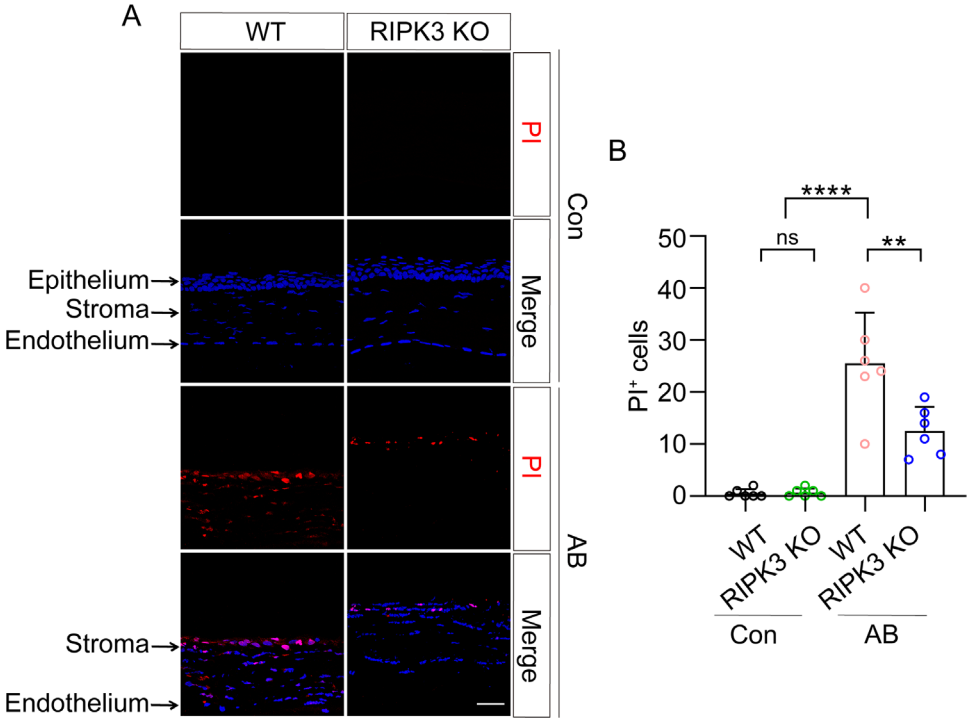

Figure 5. RIPK3 KO diminished necroptotic cell death induced by corneal AB in mice. (**A**) Representative images of PI immunofluorescence staining in each group following corneal AB. (**B**) Quantification of PI^+ cells in each group. *Blue* indicates DAPI staining. Data are presented as mean ± SEM ($n = 6$). *$P < 0.05$, **$P < 0.01$, ****$P < 0.0001$ (one-way ANOVA); ns, not significant. *Scale bar*: 20 µm.

mice exhibited a marked reduction in the number of necroptotic cells (Figs. 5A, 5B). These findings indicate that RIPK3 KO effectively diminished necroptotic cell death after AB.

RIPK3 Deficiency Inhibited MLKL-FGF2 Necroptotic Signaling

Given that RIPK3 KO mice showed a reduced number of PI^+ necroptotic cells, we further examined the role of RIPK3 in activating the downstream MLKL protein in the cornea. As shown in Figure 6A, compared to WT mice, RIPK3 KO recapitulated the inhibitory effects of p-MLKL protein after AB, but the levels of t-MLKL remained unchanged. Additionally, previous studies have indicated that the release of fibroblast growth factor 2 (FGF2) in microglia was strongly correlated with RIPK3-mediated necroptosis in OIR mice.[27] To explore the impact of AB-induced necroptosis on FGF2 regulation in the cornea, we validated these findings by assessing the induction and secretion of FGF2 from both WT and RIPK3 KO mice 5 days post-AB using immunoblot analysis. The results demonstrated that RIPK3 KO attenuated the increase in FGF2 expression. Similarly, immunofluorescence analysis confirmed that the number of $FGF2^+$ cells in $F4/80^+$ macrophages was significantly reduced in the RIPK3 KO group (Figs. 6D, 6E). Overall, these results show that RIPK3 deficiency effectively inhibited the activation of the MLKL/FGF2 pathway.

Discussion

Here, we provide mechanistic insights into severe corneal inflammation and modes of cell death after corneal AB, highlighting RIPK3 as a promising therapeutic target. Using experimental models and human frozen corneal sections from post-corneal AB patients, our study demonstrates for the first time, to our knowledge, that necroptosis is rapidly activated following AB. Notably, we observed that RIPK3 KO effectively inhibited corneal macrophage infiltration, which subsequently reduced edema, morphological damage, CoNV, and LyG driven by macrophages. Mechanistically, RIPK3 KO may suppress these pathological responses by inhibiting the MLKL/FGF2 signaling pathway in the alkali-injured cornea.

Although RIPK3 is widely recognized as a key effector in regulating cell death, particularly necroptosis, it has also been implicated in various diseases, including neurodegenerative disorders,[38] vascular conditions,[23] and inflammatory diseases.[39] Despite its established roles in these contexts, its specific function in corneal AB remains unexplored. Our study revealed significant correlations between RIPK3 activation and the upregulation of macrophage expression in post-corneal AB patients, as observed through p-RIPK3/Iba1 co-localization immunofluorescence analysis. To further validate necroptosis activation in corneal AB, we investigated the spatiotemporal expression profiles of necrosis-related proteins, including p-RIPK3, t-RIPK3, p-RIPK1, t-RIPK1, p-MLKL, and t-MLKL. Our findings revealed a rapid increase in their expression shortly after AB. Additionally, Kang et al.[40] demonstrated that RIPK3-mediated activation of necroptotic cells stimulates immune responses, where accumulated myeloid cells trigger local tissue inflammation by activating macrophages. Notably, our in vivo experiments revealed that p-RIPK3 was primarily located in $Iba1^+$ macrophages. In line with this, RIPK3–F4/80 co-localization in our study indicated high RIPK3 expression in macrophages. In light

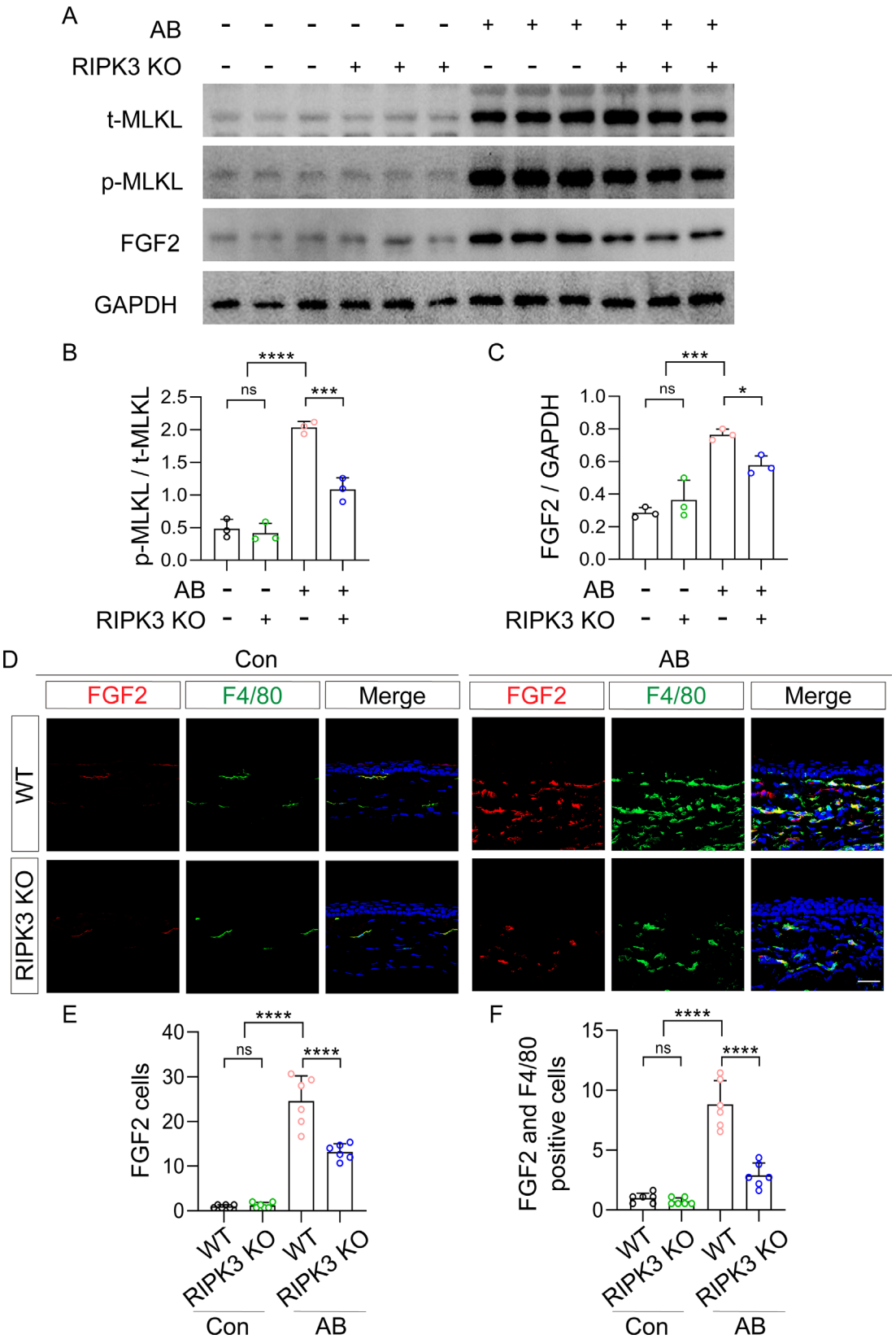

Figure 6. RIPK3 KO inhibited activation of the MLKL/FGF2 pathway in mice. (**A–C**) Western blot analysis (**A**) and densitometry analyses (**B, C**) of p-MLKL, t-MLKL, and FGF2 expression in corneal tissue from each group. Data are presented as mean ± SEM ($n = 3$). *$P < 0.05$, ***$P < 0.001$, ****$P < 0.0001$ (one-way ANOVA); ns, no significance. (**D–F**) Representative immunofluorescence images showing co-labeling of FGF2 (*red*) and F4/80 (*green*) (**D**), with quantification of FGF2$^+$ cells (**E**) and FGF2$^+$ macrophages (**F**) in each group at 3 days after corneal AB. *Blue* indicates DAPI staining. Data are presented as mean ± SEM ($n = 6$). ***$P < 0.001$, ****$P < 0.0001$ (one-way ANOVA); ns, not significant. *Scale bar*: 20 µm.

Investigative Ophthalmology & Visual Science

of these observations, necroptosis was activated and RIPK3 appears to play a pivotal role in regulating macrophage activation following AB, and RIPK3/MLKL signaling contributes to AB-induced necroptosis.

Next, we employed RIPK3 KO mice to explore the specific mechanism of the AB-induced necroptosis that triggers these events. Expectedly, our study found that RIPK3 KO significantly suppressed the intensity for RIPK3 staining in F4/80$^+$ macrophages after corneal AB. Several studies have demonstrated that necroptosis is capable of inducing inflammation infiltration,[23,24,41] which subsequently acts as a trigger for macrophage secretion.[23] In agreement with such findings, we observed macrophage production in response to acute tissue injury, whereas RIPK3 KO inhibited stromal infiltration of macrophages (CD16, CD68) in the cornea during AB, as quantified by immunofluorescence analysis. In addition to quantification of downregulation in macrophages, our H&E and AS-OCT analyses further indicated that RIPK3 KO mice exhibited reduced inflammatory cell infiltration, alleviation of corneal edema, and smaller corneal epithelial defect compared to the WT group. Our study is the first, to our knowledge, to elucidate the critical role of RIPK3 KO in mitigating macrophage-driven inflammation and preserving corneal epithelial integrity following acute alkali injury.

During the progression of corneal AB, the inflammatory response driven by extensive macrophage infiltration results in progressive corneal scarring and visual impairment.[42] Persistent macrophage infiltration induces endothelial activation, leading to vessel sprouting, formation, and subsequent remodeling.[23,43] To add to this, direct alkali injury accompanied by severe hypoxia and pH changes further exacerbates CoNV.[2] The role of necroptosis in pathological neovascularization has been demonstrated in models such as OIR,[44] where necroptosis activation promotes angiogenesis and blood vessel development.[45] In vivo, Gao et al.[46] demonstrated that RIPK3 supported angiogenesis by sustaining the expression of vascular endothelial growth factor receptor 2, further confirming that RIPK3 promotes developmental angiogenesis. In addition, LyG is closely associated with inflammation and wound healing.[47] Some macrophages have been shown to express lymphatic markers such as LYVE-1, podoplanin, and Prox-1, integrating into the vessel wall and transforming into lymphatic endothelium during inflammation.[48] Our study revealed that AB-induced necroptosis exacerbated abnormal CoNV and LyG. Importantly, RIPK3 KO effectively suppressed CoNV and LyG following macrophage infiltration. These results provide compelling evidence that RIPK3-mediated necroptosis drove CoNV and LyG by promoting macrophage infiltration after severe alkali injury.

The activation of RIPK3 and subsequent phosphorylation of MLKL are pivotal events in necroptosis.[49] RIPK3 activation triggers the formation of amyloid necrosomes, followed by MLKL oligomerization and its translocation to the cell membrane, shifting cell death from apoptosis to necroptosis.[20] During necroptosis, swollen cells and disrupted organelles cause plasma membrane rupture, which can be detected by PI staining.[37] Our study demonstrated that MLKL phosphorylation increased after AB, whereas RIPK3 KO significantly inhibited its activation and reduced PI$^+$ necroptotic cells during necroptosis induced by corneal AB. Furthermore, Orozco and Oberst[50] identified necroptotic cell death and the associated inflammation as key outcomes of RIPK3/MLKL signaling. Our immunofluorescence analysis detected that the number of FGF2$^+$ cells in F4/80$^+$ macrophages was markedly reduced by RIPK3 KO, indicating its synergistic role in promoting ocular inflammatory infiltration. Similarly, WB analysis also unveiled elevated FGF2 expression in corneal AB, which notably reduced in RIPK3 KO mice. These results suggest that RIPK3-mediated necroptosis facilitated FGF2 release, potentially acting as a downstream signaling molecule of this pathway. In addition, FGF2 functions as an endothelial cell proliferative factor and exhibits a stronger angiogenic effect.[51,52] It has been noted that necroptosis-induced retinal angiogenesis is mediated through FGF2-dependent mechanisms.[27] Based on these findings, we propose that RIPK3 KO may mitigate inflammation and CoNV by suppressing the MLKL/FGF2-mediated macrophage necroptosis.

This study is subject to several limitations that require further investigation. First, the limited sample size of human corneal specimens in our current study may restrict the ability to fully evaluate the expression and role of RIPK3 in human tissues. In future studies, we aim to increase the number of human corneal samples to better compare and validate the findings observed in the mouse model. Moreover, the present study exclusively focused on alkali injury, and it remains unclear whether RIPK3 plays a similar mediating role in other types of corneal damage or if targeting RIPK3 could alleviate other forms of corneal injury. Finally, although the animal model provided valuable insights into the underlying pathophysiology, the translation from animal studies to clinical practice remains challenging, particularly regarding the interactions between RIPK3-targeted therapies and conventional treatments, along with their safety, stability, and long-term effects in humans.

In conclusion, our study is the first, to the best of our knowledge, to identify the RIPK3-mediated macrophage necroptotic phenotype as a pivotal factor driving inflammation, pathological neovascularization, and lymphangiogenesis following corneal AB. These findings suggest that pharmacologically targeting RIPK3 could effectively disrupt the pathogenic mechanisms of AB-induced necroptosis, although its effects on cellular processes beyond necroptosis remain to be elucidated.

Acknowledgments

Supported by grants from the National Natural Science Foundation of China (82101096, 82460207); Natural Science Foundation of Guangxi Zhuang Autonomous Region (2023GXNSFAA026127, 2020GXNSFBA159015); Guangxi Science and Technology Base and Talent Special Fund (GUI KE AD20297030); and Natural Science Foundation of Guangdong Province (2025A1515012654).

Disclosure: **Y. Li**, None; **B. Yang**, None; **Q. Chen**, None; **Y. Zhou**, None; **W. Hu**, None; **X. Huang**, None; **G. Huang**, None; **N. Tang**, None; **F. Tang**, None; **H. Haung**, None; **Q. Lan**, None; **W. He**, None; **F. Xu**, None; **Y. Ye**, None; **L. Jiang**, None

References

1. Hua X, Yuan X, Li Y, et al. Desiccating stress worsens alkali burn injury by magnifying caspase-8-induced imbalance of NLRP3 and NLRP6. *J Allergy Clin Immunol.* 2017;140:1172–1176.e3.
2. Paschalis EI, Zhou C, Lei F, et al. Mechanisms of retinal damage after ocular alkali burns. *Am J Pathol.* 2017;187:1327–1342.

3. Lan C, Liu G, Huang L, et al. Forkhead domain inhibitor-6 suppresses corneal neovascularization and subsequent fibrosis after alkali burn in rats. *Invest Ophthalmol Vis Sci.* 2022;63:14.
4. Li Y, Jeong J, Song W. Molecular characteristics and distribution of adult human corneal immune cell types. *Front Immunol.* 2022;13:798346.
5. Lu P, Li L, Liu G, et al. Critical role of TNF-α-induced macrophage VEGF and iNOS production in the experimental corneal neovascularization. *Invest Ophthalmol Vis Sci.* 2012;53:3516–3526.
6. Xu J, Chen P, Luan X, et al. The NLRP3 activation in infiltrating macrophages contributes to corneal fibrosis by inducing TGF-β1 expression in the corneal epithelium. *Invest Ophthalmol Vis Sci.* 2022;63:15.
7. He L, Marneros AG. Macrophages are essential for the early wound healing response and the formation of a fibrovascular scar. *Am J Pathol.* 2013;182:2407–2417.
8. Murray PJ, Wynn TA. Protective and pathogenic functions of macrophage subsets. *Nat Rev Immunol.* 2011;11:723–737.
9. Robinson N, Ganesan R, Hegedűs C, Kovács K, Kufer TA, Virág L. Programmed necrotic cell death of macrophages: focus on pyroptosis, necroptosis, and parthanatos. *Redox Biol.* 2019;26:101239.
10. Guo X-X, Pu Q, Hu J-J, Chang X-J, Li A-L, Li X-Y. The role of regulated necrosis in inflammation and ocular surface diseases. *Exp Eye Res.* 2023;233:109537.
11. Aebischer D, Lolyeva M, Halin C. The inflammatory response of lymphatic endothelium. *Angiogenesis.* 2014;17:383–393.
12. Halin C, Tobler NE, Vigl B. VEGF-A produced by chronically inflamed tissue induces lymphangiogenesis in draining lymph nodes. *Blood.* 2017;110:3158–3167.
13. Huggenberger R, Siddiqui SS, Brander D, et al. An important role of lymphatic vessel activation in limiting acute inflammation. *Blood.* 2011;117:4667–4678.
14. Tuft SJ, Shortt AJ. Surgical rehabilitation following severe ocular burns. *Eye (Lond).* 2009;23:1966–1971.
15. Clare G, Bunce C, Tuft S. Amniotic membrane transplantation for acute ocular burns. *Cochrane Database Syst Rev.* 2022;9:CD009379.
16. Sharma N, Kaur M, Agarwal T. Treatment of acute ocular chemical burns. *Surv Ophthalmol.* 2018;63:214–235.
17. Sun L, Wang H, Wang Z, et al. Mixed lineage kinase domain-like protein mediates necrosis signaling downstream of RIP3 kinase. *Cell.* 2012;148:213–227.
18. Newton K, Dugger DL, Wickliffe KE, et al. Activity of protein kinase RIPK3 determines whether cells die by necroptosis or apoptosis. *Science.* 2014;343:1357–1360.
19. Cho YS, Challa S, Moquin D, et al. Phosphorylation-driven assembly of the RIP1–RIP3 complex regulates programmed necrosis and virus-induced inflammation. *Cell.* 2009;137:1112–1123.
20. Li J, McQuade T, Siemer AB, et al. The RIP1/RIP3 necrosome forms a functional amyloid signaling complex required for programmed necrosis. *Cell.* 2012;150:339–350.
21. Murphy JM, Czabotar PE, Hildebrand JM, et al. The pseudokinase MLKL mediates necroptosis via a molecular switch mechanism. *Immunity.* 2013;39:443–453.
22. Hu H, Wu X, Wu G, et al. RIP3-mediated necroptosis is regulated by inter-filament assembly of RIP homotypic interaction motif. *Cell Death Differ.* 2021;28:251–266.
23. Ueta T, Ishihara K, Notomi S, et al. RIP1 kinase mediates angiogenesis by modulating macrophages in experimental neovascularization. *Proc Natl Acad Sci USA.* 2019;116:23705–23713.
24. Zeng X, Zhang Y-D, Ma R-Y, et al. Activated Drp1 regulates p62-mediated autophagic flux and aggravates inflammation in cerebral ischemia-reperfusion via the ROS-RIP1/RIP3-exosome axis. *Mil Med Res.* 2022;9:25.
25. Cao L, Mu W. Necrostatin-1 and necroptosis inhibition: pathophysiology and therapeutic implications. *Pharmacol Res.* 2021;163:105297.
26. Karunakaran D, Geoffrion M, Wei LH, et al. Targeting macrophage necroptosis for therapeutic and diagnostic interventions in atherosclerosis. *Sci Adv.* 2016;2:e1600224.
27. He C, Liu Y, Huang Z, et al. A specific RIP3$^+$ subpopulation of microglia promotes retinopathy through a hypoxia-triggered necroptotic mechanism. *Proc Natl Acad Sci USA.* 2021;118:e2023290118.
28. Yu Z, Efstathiou NE, Correa VS, et al. Receptor interacting protein 3 kinase, not 1 kinase, through MLKL-mediated necroptosis is involved in UVA-induced corneal endothelium cell death. *Cell Death Discov.* 2021;7:366.
29. You X-G, Fan T-J, Jiang G-J. Phenylephrine induces necroptosis and apoptosis in corneal epithelial cells dose- and time-dependently. *Toxicology.* 2019;428:152305.
30. Nominato LF, Dias AC, Dias LC, et al. Prevention of corneal neovascularization by adenovirus encoding human vascular endothelial growth factor soluble receptor (s-VEGFR1) in lacrimal gland. *Invest Ophthalmol Vis Sci.* 2018;59:6036–6044.
31. Zhou C, Robert M-C, Kapoulea V, et al. Sustained subconjunctival delivery of infliximab protects the cornea and retina following alkali burn to the eye. *Invest Ophthalmol Vis Sci.* 2017;58:96–105.
32. Baradaran-Rafii A, Eslani M, Haq Z, Shirzadeh E, Huvard MJ, Djalilian AR. Current and upcoming therapies for ocular surface chemical injuries. *Ocul Surf.* 2017;15:48–64.
33. Flister MJ, Wilber A, Hall KL, et al. Inflammation induces lymphangiogenesis through up-regulation of VEGFR-3 mediated by NF-κB and Prox1. *Blood.* 2010;115:418–429.
34. Clahsen T, Hadrian K, Notara M, et al. The novel role of lymphatic vessels in the pathogenesis of ocular diseases. *Prog Retin Eye Res.* 2023;96:101157.
35. Chinnery HR, McMenamin PG, Dando SJ. Macrophage physiology in the eye. *Pflügers Arch.* 2017;469:501–515.
36. Kataru RP, Jung K, Jang C, et al. Critical role of CD11b$^+$ macrophages and VEGF in inflammatory lymphangiogenesis, antigen clearance, and inflammation resolution. *Blood.* 2009;113:5650–5659.
37. Unal Cevik I, Dalkara T. Intravenously administered propidium iodide labels necrotic cells in the intact mouse brain after injury. *Cell Death Differ.* 2003;10:928–929.
38. Murakami Y, Matsumoto H, Roh M, et al. Receptor interacting protein kinase mediates necrotic cone but not rod cell death in a mouse model of inherited degeneration. *Proc Natl Acad Sci USA.* 2012;109:14598–14603.
39. Huang D, Chen P, Huang G, et al. Salt-inducible kinases inhibitor HG-9-91-01 targets RIPK3 kinase activity to alleviate necroptosis-mediated inflammatory injury. *Cell Death Dis.* 2022;13:188.
40. Kang YJ, Bang B-R, Han KH, et al. Regulation of NKT cell-mediated immune responses to tumours and liver inflammation by mitochondrial PGAM5-Drp1 signalling. *Nat Commun.* 2015;6:8371.
41. Gautam A, Boyd DF, Nikhar S, et al. Necroptosis blockade prevents lung injury in severe influenza. *Nature.* 2024;628:835–843.
42. Li Q, Hua X, Li L, et al. AIP1 suppresses neovascularization by inhibiting the NOX4-induced NLRP3/NLRP6 imbalance in a murine corneal alkali burn model. *Cell Commun Signal.* 2022;20:59.
43. Arroyo AG, Iruela-Arispe ML. Extracellular matrix, inflammation, and the angiogenic response. *Cardiovasc Res.* 2010;86:226–235.

Investigative Ophthalmology & Visual Science

44. Ni B, Yang Z, Zhou T, et al. Therapeutic intervention in neuroinflammation for neovascular ocular diseases through targeting the cGAS–STING–necroptosis pathway. *J Neuroinflammation*. 2024;21:164.
45. Tisch N, Freire-Valls A, Yerbes R, et al. Caspase-8 modulates physiological and pathological angiogenesis during retina development. *J Clin Invest*. 2019;129:5092–5107.
46. Gao S, Griffin CT. RIPK3 modulates growth factor receptor expression in endothelial cells to support angiogenesis. *Angiogenesis*. 2021;24:5092.
47. Seo M, Choi JS, Rho CR, Joo C-K, Lee SK. MicroRNA miR-466 inhibits lymphangiogenesis by targeting prospero-related homeobox 1 in the alkali burn corneal injury model. *J Biomed Sci*. 2015;22:3.
48. Hori J, Yamaguchi T, Keino H, Hamrah P, Maruyama K. Immune privilege in corneal transplantation. *Prog Retin Eye Res*. 2019;72:100758.
49. Zhao J, Jitkaew S, Cai Z, et al. Mixed lineage kinase domain-like is a key receptor interacting protein 3 downstream component of TNF-induced necrosis. *Proc Natl Acad Sci USA*. 2012;109:5322–5327.
50. Orozco S, Oberst A. RIPK3 in cell death and inflammation: the good, the bad, and the ugly. *Immunol Rev*. 2017;277:102–112.
51. Cao R, Eriksson A, Kubo H, Alitalo K, Cao Y, Thyberg J. Comparative evaluation of FGF-2-, VEGF-A-, and VEGF-C–induced angiogenesis, lymphangiogenesis, vascular fenestrations, and permeability. *Circ Res*. 2004;94:664–670.
52. Cross MJ, Claesson-Welsh L. FGF and VEGF function in angiogenesis: signalling pathways, biological responses and therapeutic inhibition. *Trends Pharmacol Sci*. 2001;22:201–207.

Investigative Ophthalmology & Visual Science